An Optimized Ultraviolet-A Light Photodetector with Wide-Range Photoresponse Based on ZnS/ZnO Biaxial Nanobelt

*Linfeng Hu, Jian Yan, Meiyong Liao, Hongjun Xiang, Xingao Gong, Lide Zhang, and Xiaosheng Fang**

One-dimensional (1D) semiconductor nanostructures are considered as the most promising sensitive materials in photodetectors due to the large surface-to-volume ratio and a Debye length comparable to their small size for the 1D semiconductor nanostructures.[1] Generally, the large surface-to-volume ratio can significantly increase the number of surface trap states and prolong the photocarrier lifetime; and the reduced dimensionality can confine the active area of the charge carrier and shorten the transit time.[2] Therefore, the photodetectors constructed from 1D semiconductor nanostructures usually show high sensitivity,[3] high quantum efficiency,[4] or fast response speed.[5]

It is known that the ultraviolet (UV) radiation emitted by the sun falls in the range 200–400 nm. Most of UV-C (200–290 nm) light and UV-B (290–320 nm) light can be absorbed by the molecules in sunscreen lotions and the Earth's atmosphere, respectively, and UV-A (320–400 nm) light can reach the earth's surface leading to skin cancer. Although a large variety of photodetectors from 1D semiconductor nanostructures have been widely reported, there have been rather limited researches on the photon detection of UV-A light. ZnO and ZnS (cubic zinc blende (ZB), and hexagonal wurtzite (WZ)), well-known direct bandgap II–VI semiconductors with room-temperature bandgaps of ~3.37 eV (WZ-ZnO), ~3.29 eV (ZB-ZnO), ~3.77 eV (WZ-ZnS), and ~3.72 eV (ZB-ZnS), are the most important materials for UV-A light photodetectors.[6] Nevertheless, the UV-A light photodetectors based on ZnO nanostructures mostly exhibit a slow response speed and poor photocurrent stability due to the inherent defects such as oxygen vacancies and zinc interstitials.[7] The UV-A light photodetectors constructed from ZnS nanostructures also show weak photocurrent and unsatisfactory stability.[6b] Therefore, it is crucial and highly desired to develop novel photodetectors to effectively detect UV-A irradiation.

Semiconducting nanocomposites consisting of several different functional materials have attracted considerable attention for the possible use in the electronic and optoelectronic devices due to their multifunctions. Recently, we have successfully synthesized side-to-side single-crystalline ZnS/ZnO biaxial nanobelts via a simple thermal evaporation method.[8] We expect that these ZnS/ZnO biaxial nanobelts may be very promising candidates for UV A-light sensors due to their binary composition. In this communication, we have successfully developed an UV-A light photodetector from this ZnS/ZnO biaxial nanobelt. To the best of our knowledge, this is the first study on the optoelectronic device of 1D semiconductor/semiconductor nanocomposites. Our photodetector based on this binary ZnS/ZnO biaxial nanobelt exhibits tunable spectral selectivity and wide-range photoresponse for the UV-A band. More importantly, the optimized performance of this ZnS/ZnO photodetector is much better than that of pure ZnS or ZnO nanostructures through combining the wide-range UV-A light photoresponse, high sensitivity, and very fast response speed.

The ZnS/ZnO biaxial nanobelts were grown by the routes described in our previous study.[8] **Figure 1**a is the typical scanning electron microscopy (SEM) images of the as-grown ZnS/ZnO nanobelts. The substrate is densely covered by a large scale of ZnS/ZnO biaxial nanobelts with diameters varying from several tens of nm to 100 nm and lengths up to tens of micrometers. SEM image at high magnification of a bending ZnS/ZnO nanobelt are inserted in Figure 1a. Our previous study suggests that the curving of the ZnS/ZnO biaxial nanobelt should be attributed to the mismatch stress between the ZnS and ZnO lattices.[8] Further observation by transmission electron microscopy (TEM) indicates that most of the nanobelt is composed of two sides with different bright/dark colors, as shown in Figure 1b. From the high-resolution transmission electron microscopy (HRTEM) image in Figure 1c, one can see a distinct interface between two parallel layers for an individual nanobelt, corresponding to the WZ ZnS single-crystalline side and WZ ZnO single-crystalline side. The marked inter-planar *d* spacings, 0.62 nm and 0.52 nm in each side, respectively correspond to the (0001) planes of WZ ZnS and (0001) plane of WZ ZnO. The clear lattice fringes observed in the HRTEM

Dr. L. F. Hu, Prof. X. S. Fang
Department of Materials Science
Fudan University
Shanghai 200433, PR China
E-mail: xshfang@fudan.edu.cn
Dr. J. Yan, Prof. L. D. Zhang
Key Laboratory of Materials Physics and Anhui Key Laboratory of Nanomaterials and Nanostructures
Institute of Solid State Physics
Hefei Institutes of Physical Science
Chinese Academy of Sciences
Hefei 230031, PR China
Dr. M. Y. Liao
Optical and Electronic Materials Unit
National Institute for Materials Science (NIMS)
Namiki 1-1, Tsukuba, Ibaraki 305-0044, Japan
Prof. H. J. Xiang, Prof. X. G. Gong
Key Laboratory of Computational Physical Sciences (Ministry of Education) and Department of Physics
Fudan University
Shanghai 200433, PR China

DOI: 10.1002/adma.201200512

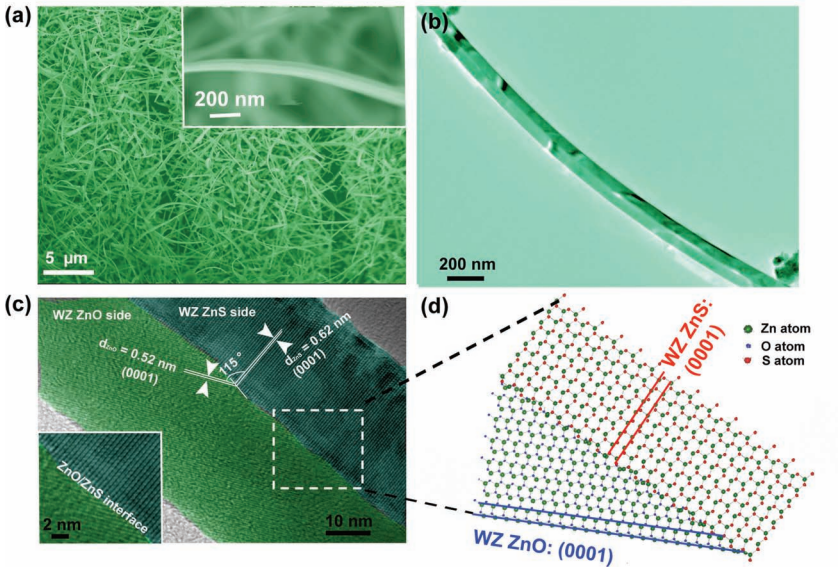

Figure 1. a) Typical SEM images of the as-grown ZnS/ZnO biaxial nanobelts on a Si (100) substrate with the high-magnification SEM image inserted. b) TEM and c) HRTEM images of the ZnS/ZnO biaxial nanobelts with the enlarged portion inserted. The ZnS and ZnO sides in (c) are distinguished by two different colors. d) Atomic structural model of the ZnS/ZnO interface viewed along the [100] direction.

image demonstrate the superior crystal quality on both the ZnS single-crystalline side and ZnO single-crystalline side. An angle between these two crystal planes can be observed at 115° from the HRTEM image, and the interface between the WZ ZnS side and the WZ ZnO side is atomically smooth. The atomic configuration of the top surface of our ZnS/ZnO biaxial nanobelt illustrated in Figure 1d shows the hetero-crystalline structure with ZnO (0001)/ZnS(0001) interface.

An individual ZnS/ZnO nanobelt-based photodetector was then constructed by standard lithography procedures. As shown in **Figure 2**a, a pair of 10 nm/100 nm Cr/Au electrodes with 3 μm apart is deposited on the ZnS/ZnO nanobelt dispersed at a SiO_2/Si substrate (denoted as device I). The current–voltage (I–V) curves of the device in Figure 2b indicates that the device current across the ZnS/ZnO nanobelt increases remarkably from 0.67 μA (dark condition) to 4.64 μA under 320 nm-light illumination (0.91 mW cm^{-2}) at an applied voltage of 5.0 V. It should be noteworthy that I–V curves are linear and symmetric, suggesting the good ohmic contact between the ZnS/ZnO nanobelt and the Cr/Au electrodes. This result is quite different with the rectification curves which are usually observed in some nanowire heterojunction-based photodetectors.[9] Although our ZnS/ZnO biaxial nanobelt can be considered as a heterostructure, the as-observed ohmic behavior of the device demonstrates that no free carriers are trapped and blocked at the ZnS/ZnO interface of the biaxial nanobelt. The electrical transport characteristics of our ZnS/ZnO nanobelts were further measured based on bottom-gate ZnS/ZnO nanobelt field-effect transistors (FETs) as shown in Supporting Information (SI) Figure S1a. The source–drain current of the FETs decreases as the gate voltage (I_{ds}-V_{ds}) decreases (SI, Figure S1b), exhibiting typical n-type semiconductor characteristics.[10] Accordingly, the majority carriers of the present ZnS/ZnO nanobelt device are electrons rather than holes, which should be due to the presence of intrinsic donor-type defects induced by deviations from stoichiometry between Zn and O,S components during the synthesis of the ZnS/ZnO biaxial nanobelts.[11]

Figure 2c depicts the photon-response spectra of the device as a function of the incident light wavelength at a bias of 1.0 V. The sensitivity is very low when the wavelength is higher than 400 nm, and gradually increases by about four orders of magnitude when the device is illuminated by a light with energy above this threshold wavelength. As expected, an increase step can be clearly observed between 300 to 400 nm wavelength ranges. The first increase of photon response between 348 and 400 nm shows threshold excitation energy of ≈3.4 eV (370 nm), closing to the bandgap energy of ZnO, and the second increase from 300 to 348 nm can be attributed to the excitation of electron–hole pairs by the incident light with energy larger than the bandgap of ZnS. It should be noteworthy that another absorption peak at around 270 nm (4.6 eV) is observed in Figure 2c. The origin of this peak is still not so clear, and we speculate that it might be attributed to the charge transfer from the ZnO valence band to the ZnS conduction band. Therefore, these results confirm that the performance of the present device combines the optoelectronic signals from both the ZnS and ZnO. The tuned sensitive wavelength region for our ZnS/ZnO nanobelt from 300 to 400 nm is well consistent with that of the UV-A band. Compared with the previously reported UV-A photodetectors which shows very low photoresponse at low wavelength range,[12] the present photodetector based on the biaxial ZnS/ZnO nanobelt with wide-range photoresponse is more suitable for UV light detection.

Generally, the spectra responsivity (R_λ) and external quantum efficiency (EQE) are two critical parameters to determine the sensitivity for an optoelectronic device.[13] R_λ is defined as the photocurrent generated per unit power of incident light on the effective area of a photoconductor, and EQE is related to the number of electron-hole pairs excited by one absorbed photon. R_λ and EQE can be expressed as $R_\lambda = \frac{\Delta I}{PS}$ and $EQE = \frac{hc}{e\lambda} \cdot \frac{\Delta I}{PS}$, respectively.[14] Wherein, ΔI is the difference between photo-excited current and dark current, P is the light power density irradiated on the nanobelt, and S is the irradiated area of an individual nanobelt, λ is the exciting wavelength, h is Planck's constant, c is the velocity of the light, and e is the electronic charge. The calculated R_λ and EQE values of the present ZnS/ZnO biaxial nanobelt are as high as 5.0×10^5 A/W and 2.0×10^8% irradiated by 320 nm light at an applied voltage of 5.0 V, respectively. Such an ultrahigh value of R_λ or EQE indicates high UV-A light sensitivity of the present device.

Repeatability and response speed are the key parameters to determine the capability of a photodetector. It is still a challenge to achieve photodetectors with both high sensitivity and fast temporal response up to date. The excellent repeatability of

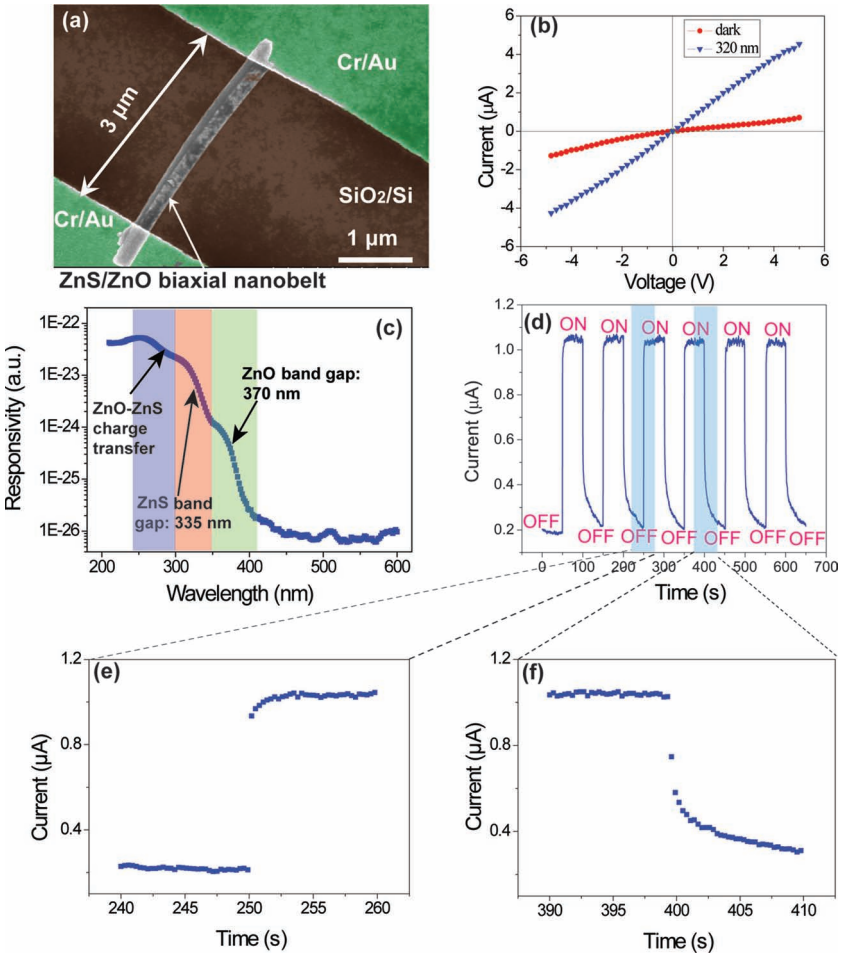

Figure 2. a) A representative SEM image of the photodetector based on ZnS/ZnO biaxial nanobelt with Cr/Au electrodes deposition at the two ends. b) *I–V* curves under dark condition and UV-light illumination. c) Spectral photoresponse measured from the UV-light device at a bias of 5.0 V. d) The reproducible on/off switching of the device upon 320 nm light illumination with a ~50 s cycle at a bias of 1.0 V. e,f) The enlarged portions of a 240–260 s range and a 390–410 s range corresponding to light-off to light-on and light-on to light-off transitions, respectively.

the present ZnS/ZnO nanobelt device has been checked over 50 turning switching on/off cycles under 320 nm light illumination at a bias of 1.0 V. As shown in Figure 2d, with the light irradiation on and off, the current of the device mostly exhibits two distinct states, a low-current state of 0.2 μA in the dark and a high-current state of 1.0 μA under light illumination. The current increases very sharply from one state to another state, indicating a very fast response speed of the device. The very fast response speed is further confirmed by the enlarged portions of a 240–260 s range and a 390–410 s range corresponding to the low-current state and the high-current state, respectively, as shown in Figure 2e,f. One can see that the rise time is faster than the limit of our measurement setup (0.3 s). The decaying edges of the photocurrents in Figure 2f can be well fitted by the exponential equation $I = I_0 e^{-t/\tau d}$, and the decay time τ_d can be estimated to ~1.7 s.

To examine the reproducibility of the optoelectronic behavior for our ZnS/ZnO biaxial nanobelts, about 20 photodetectors have been fabricated using the same routes. The SEM morphology and the UV photoresponse results of another device (denoted as device II) are shown in SI, Figure S2 and S3, respectively. From Figure S3a, one can see that the device II displays the similar UV-light sensitive behaviors compared with device I. The photocurrent exhibits a slight increase with the illumination of visible light (λ > 400 nm) and a drastic increment under UV-A light (320 nm), confirming the excellent repeatability of our ZnS/ZnO nanobelt photodetectors. The photocurrent of device II (17.7 μA) is larger than that of device I (5.0 μA) under the same measurement conditions (320 nm-light illumination, an applied voltage of 5.0 V), and it should be ascribed to the presence of geometric difference between the nanobelts in these two devices. The photoresponse under various environments were further examined as shown in SI, Figure S3b. The result indicates that the photocurrent apparently increases from 17.7 to 45.2 μA with decreasing the gas pressure of the measurement environment to 0.5 Pa. Such a result has been frequently observed in previous study, and the reason should be attributed to the existence of the oxygen chemisorption/desorption on the ZnS/ZnO nanobelt surface. Due to the large surface-to-volume ratio of the 1D ZnS/ZnO nanobelt, oxygen molecules are adsorbed on the nanobelt surface creating a depletion layer with low conductivity [$O_{2(gas)} + e^- \rightarrow O_2^-{}_{(adsorption)}$]. Upon illumination, the photogenerated holes move to the surface along the potential gradient produced by band-bending and desorb oxygen from the surface, resulting in an increase in the free carrier concentration and a decrease in the width of the depletion layer [$h^+ + O_2^-{}_{(adsorption)} \rightarrow O_{2(gas)}$]. Under vacuum condition, oxygen desorption becomes more prominent, and therefore the concentration of free carriers is higher in vacuum than in air.[4]

As summarized in **Table 1**, the performance of the present ZnS/ZnO biaxial nanobelt photodetector is significantly enhanced compared with that of pure ZnS or ZnO nanostructures by combining the high UV-A light sensitivity and fast response speed, justifying the effective utilization of the present ZnS/ZnO biaxial nanobelt as the building blocks of UV photodetectors. Interestingly, the photocurrent of our device is about 10^3 and 10^6 times higher than that of the device constructed from pure ZnS nanobelt and ZnO nanowire, respectively, and also much higher than that of the summation of photocurrents from both pure ZnS and ZnO nanostructures. Although the reason for this remarkable enhancement is not quite clear, we propose that it may be understood from the band energy alignment of the ZnS/ZnO biaxial nanobelts. As shown in **Figure 3**, the position of the valence-band energy level in ZnS is 0.8 eV higher than that of ZnO, and a type-II heterostructure

Table 1. Comparison of the characteristic parameters of ZnS/ZnO biaxial nanobelt photodetector and pure ZnS, ZnO photodetectors.

Photodetectors	Dark current	Photocurrent	*EQE* [%]	Rise time	Decay time	Reference
ZnO nanowire	0.13 pA (at 1.0 V)	0.13 nA (at 1.0 V)	—	40 s	300 s	[7a]
ZnO nanowire	~15 pA (at 5.0 V)	0.28 nA (at 5.0 V)	—	43.7 s	—	[7b]
ZnS nanobelt	<1 pA (at 5.0 V)	1 pA (at 5.0 V)	50 (at 5.0 V)	<0.3 s	<0.3 s	[6c]
ZnS-coated ZnO arrays	1.62 mA (at 3.0 V)	—	—	229 s	547 s	[17a]
SnO_2-coated ZnO nanowire composites	~31 nA (at 0.8 V)	~140 n A (at 0.8V)	—	1.5 s	~25.6 s	[17c]
ZnS/ZnO nanobelt (Device I)	0.67 μA (at 5.0 V)	4.64 μA (at 5.0 V)	2×10^8 (at 5.0 V)	<0.3 s	1.7 s	This work
ZnS/ZnO nanobelt (Device II)	3.03 μA (at 5.0 V)	17.76 μA (at 5.0 V)	7.4×10^8 (at 5.0 V)	<0.3 s	1.5 s	This work

with a staggered alignment at the heterjunction is formed for our ZnS/ZnO biaxial nanobelts.[15] In this case, following the generation of electron–hole pairs under light illumination, the electrons will move to the ZnO side and holes will move to the ZnS side due to the internal field at the ZnS/ZnO interface, facilitating the formation of a charge transfer state and the spatial separation of the photogenerated carriers within the nanobelts.[16] The spatial separation of the photogenerated carriers can decrease the recombination of the electron–hole pairs, and therefore significantly increase the photocurrent and *EQE* value of the present ZnS/ZnO nanobelt device. Furthermore, the good ohmic contact with no interfacial barrier or traps between the ZnS/ZnO nanobelt and the Cr/Au electrodes should also be responsible for the high photocurrent of the present device. On the other hand, since the electrons and the holes are separated in the ZnO side and the ZnS side, respectively, the high carries mobility in the high-crystalline ZnS/ZnO nanobelt might lead to the recombination of partial electron–hole pairs at the Cr/Au electrodes rather than on the nanobelt surface through the aforementioned oxygen absorption-desorption processes.[4] This makes sure the excellent transient response behavior and fast response speed of our device due to that hole diffusion and oxygen desorption process generally results in a slow response speed.[7a]

Such an enhancement effect has also been observed in ZnS-coated ZnO nanowire arrays and SnO_2-coated ZnO nanowire composites.[17] However, the response speed of those devices is much slower than that of our device. The reason may be understood by the fact that the ZnS or SnO_2 layer on the ZnO nanowire surface act as a shielding layer and leads to a low photoexcitation. In contrast, our ZnS/ZnO biaxial nanobelts expose both ZnO and ZnS surface, ensuring the maximum absorption of UV light.

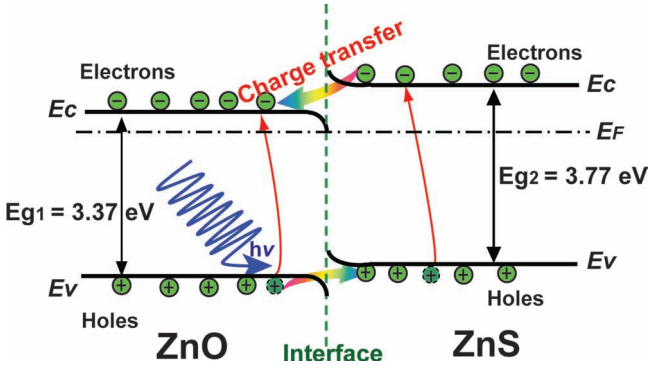

Figure 3. Schematic energy band diagram for ZnS/ZnO biaxial nanobelt after UV irradiation.

In conclusion, for the first time, we have developed a novel 1D/1D semiconductor/semiconductor nanocomposite-based photodetector from high-crystallized ZnS/ZnO biaxial nanobelts. The as-developed photodetector exhibits high spectral selectivity and wide-range photoresponse on UV-A band. The optimized performance of our photodetector based on this binary ZnS/ZnO biaxial nanobelt is much better than that of pure ZnS or ZnO nanostructures and nanoparticle-coated ZnO composites through combining the high sensitivity, *EQE* value and fast response speed. This photodetector is particularly suitable for UV-A light detection, and its fast response speed also enables great application potential on high-frequency light-wave communications, photoelectronic switches, future memory storage, and optoelectronic circuits. Further study is still underway to develop various novel photodetctors using the similar approach based on other 1D semiconductor/semiconductor nanocomposites.

Experimental Section

ZnS/ZnO biaxial nanobelts were synthesized by a thermal evaporation method similar to that in our previous reports.[8] An individual ZnS/ZnO biaxial nanobelt was assembled as a nanoscale photodetector by standard lithography procedures. The current–voltage (*I–V*) characteristics of the ZnS/ZnO biaxial nanobelt photodetector were measured using an Advantest Picoammeter R8340A and a DC voltage source R6411 (see SI for details).

Supporting Information

Supporting Information is available from the Wiley Online Library or from the author.

Acknowledgements

LFH and JY contributed equally to this work. This work was supported by the National Natural Science Foundation of China (Grant Nos. 91123006, 21001028 and 51002032), the National Basic Research Program of China (Grant No. 2012CB932303), Shanghai Chenguang Foundation (11CG06), Shanghai Pujiang Program (11PJ1400300), Science and Technology Commission of Shanghai Municipality (11520706200), and

the Programs for Professor of Special Appointment (Eastern Scholar) at Shanghai Institutions of Higher Learning and for New Century Excellent Talents in University (NCET-11-0102).

Received: February 6, 2012
Published online: March 30, 2012

[1] a) C. M. Lieber, Z. L. Wang, *MRS Bull.* **2007**, *32*, 99; b) H. Kind, H. Yan, B. Messer, M. Law, P. D. Yang, *Adv. Mater.* **2002**, *14*, 158; c) L. Li, Y. W. Yang, G. H. Li, L. D. Zhang, *Small* **2006**, *2*, 548.
[2] S. Liu, J. F. Ye, Y. Cao, Q. Shen, Z. F. Liu, L. M. Qi, X. F. Guo, *Small* **2009**, *5*, 2371.
[3] C. Soci, A. Zhang, B. Xiang, S. A. Dayeh, D. P. R. Aplin, J. Park, X. Y. Bao, Y. H. Lo, D. Wang, *Nano Lett.* **2007**, *7*, 1003.
[4] a) L. Li, X. S. Fang, T. Y. Zhai, M. Y. Liao, U. K. Guatam, X. C. Wu, Y. Koide, Y. Bando, D. Golberg, *Adv. Mater.* **2010**, *22*, 4151; b) L. F. Hu, J. Yan, M. Y. Liao, L. M. Wu, X. S. Fang, *Small* **2011**, *7*, 1012.
[5] a) S. C. Kung, W. E. van der Veer, F. Yang, K. C. Donavan, R. M. Penner, *Nano Lett.* **2010**, *10*, 1481; b) L. F. Hu, L. M. Wu, M. Y. Liao, X. S. Fang, *Adv. Mater.* **2011**, *23*, 1988.
[6] a) C. Y. Yeh, S. H. Wei, A. Zunger, *Phys. Rev. B* **1994**, *50*, 2715; b) C. S. Lao, M. C. Park, Q. Kuang, Y. L. Deng, A. K. Sood, D. L. Polla, Z. L. Wang, *J. Am. Chem. Soc.* **2007**, *129*, 12096; c) X. S. Fang, Y. Bando, M. Y. Liao, U. K. Gautam, C. Y. Zhi, B. Dierre, B. D. Liu, T. Y. Zhai, T. Sekiguchi, Y. Koide, D. Golberg, *Adv. Mater.* **2009**, *21*, 2034.
[7] a) K. W. Liu, M. Sakurai, M. Y. Liao, M. Aono, *J. Phys. Chem. C* **2010**, *114*, 19835; b) S. E. Ahn, H. J. Ji, K. Kim, G. T. Kim, C. H. Bae, S. M. Park, Y. K. Kim, J. S. Ha, *Appl. Phys. Lett.* **2007**, *90*, 153106.
[8] J. Yan, X. S. Fang, L. D. Zhang, Y. Bando, U. K. Gautam, B. Dierre, T. Sekiguchi, D. Golberg, *Nano Lett.* **2008**, *8*, 2794.
[9] H. W. Lin, H. B. Liu, X. M. Qian, S.-W. Lai, Y. J. Li, N. Chen, C. B. Ouyang, C. M. Che, Y. L. Li, *Inorg. Chem.* **2011**, *50*, 7749.
[10] S. S. Kwon, W. K. Hong, G. Jo, J. Maeng, T. W. Kim, S. Song, T. Lee, *Adv. Mater.* **2008**, *20*, 4557.
[11] D. C. Look, J. W. Hemsky, J. R. Sizelove, *Phys. Rev. Lett.* **1999**, *82*, 2552.
[12] L. W. Sang, M. Y. Liao, Y. Koide, M. Sumiya, *Appl. Phys. Lett.* **2011**, *98*, 103502.
[13] G. Konstantatos, E. H. Sargent, *Nat. Nanotechnol.* **2010**, *5*, 391.
[14] L. Li, P. C. Wu, X. S. Fang, T. Y. Zhai, L. Dai, M. Y. Liao, Y. Koide, H. Q. Wang, Y. Bando, D. Golberg, *Adv. Mater.* **2010**, *22*, 3161.
[15] Y. H. Li, A. Walsh, S. Y. Chen, W. J. Yin, J. H. Yang, J. B. Li, J. D. Ailva, X. G. Gong, S. H. Wei, *Appl. Phys. Lett.* **2009**, *94*, 212109.
[16] S. S. Lo, T. Mirkovic, C. H. Chuang, C. Burda, G. D. Scholes, *Adv. Mater.* **2011**, *23*, 180.
[17] a) A. Bera, D. Basak, *ACS Appl. Mater. Interfaces* **2010**, *2*, 408; b) K. Wang, J. J. Chen, Z. M. Zeng, J. Tarr, W. L. Zhou, Y. Zhang, Y. F. Yan, C. S. Jiang, J. Pern, A. Mascarenhas, *Appl. Phys. Lett.* **2010**, *96*, 123105; c) C. C. Lin, Y. W. Chen, M. C. Chiang, C. H. Lee, Y. L. Tung, S. Y. Chen, *J. Electochem. Soc.* **2010**, *157*, H227.